Science of the Total Environment 628–629 (2018) 815–825

Contents lists available at ScienceDirect

Science of the Total Environment

journal homepage: www.elsevier.com/locate/scitotenv

Downscaling hydrodynamics features to depict causes of major productivity of Sicilian-Maltese area and implications for resource management

Fulvio Capodici [a,*], Giuseppe Ciraolo [a], Simone Cosoli [b], Antonino Maltese [a], M. Cristina Mangano [c], Gianluca Sarà [c]

[a] Dipartimento di Ingegneria Civile Ambientale, Aerospaziale, dei Materiali, Università degli Studi di Palermo, Bld. 8 Viale delle Scienze, Palermo, Italy
[b] Ocean Graduate School and the Oceans Institute, The University of Western Australia, 35 Stirling Highway Perth, Crawley, WA 6009, Australia
[c] Dipartimento di Scienze della Terra e del mare, DiSTeM, Università degli Studi di Palermo, Viale delle Scienze Ed. 16, 90128 Palermo, Italy

HIGHLIGHTS

- The correlation between HF currents, CHL-*a* and SST satellite data is proposed.
- High temporal HF radar data is used to resolve the main oceanographic features.
- Correlation maps allow to disentangle how sea current-driven CHL-*a* and SST affect biological and ecological processes

GRAPHICAL ABSTRACT

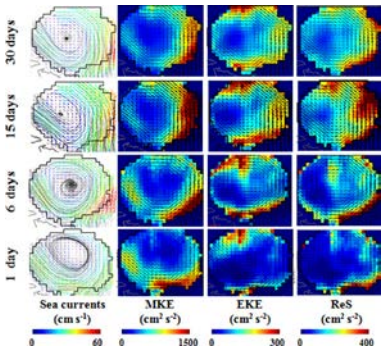

ARTICLE INFO

Article history:
Received 3 December 2017
Received in revised form 9 February 2018
Accepted 9 February 2018
Available online xxxx

Editor: D. Barcelo

Keywords:
SST
CHL-a
HF radars
Sea surface currents
Spatial correlation
Biology

ABSTRACT

Chlorophyll-*a* (*CHL-a*) and sea surface temperature (*SST*) are generally accepted as proxies for water quality. They can be easily retrieved in a quasi-near real time mode through satellite remote sensing and, as such, they provide an overview of the water quality on a synoptic scale in open waters. Their distributions evolve in space and time in response to local and remote forcing, such as winds and currents, which however have much finer temporal and spatial scales than those resolvable by satellites in spite of recent advances in satellite remote-sensing techniques. Satellite data are often characterized by a moderate temporal resolution to adequately catch the actual sub-grid physical processes. Conventional pointwise measurements can resolve high-frequency motions such as tides or high-frequency wind-driven currents, however they are inadequate to resolve their spatial variability over wide areas. We show in this paper that a combined use of near-surface currents, available through High-Frequency (HF) radars, and satellite data (*e.g.*, TERRA and AQUA/MODIS), can properly resolve the main oceanographic features in both coastal and open-sea regions, particularly at the coastal boundaries where satellite imageries fail, and are complementary tools to interpret ocean productivity and resource management in the Sicily Channel.

* Corresponding author.
E-mail addresses: fulvio.capodici@unipa.it (F. Capodici), giuseppe.ciraolo@unipa.it (G. Ciraolo), simone.cosoli@uwa.edu.au (S. Cosoli), antonino.maltese@unipa.it (A. Maltese), mariacristina.mangano01@unipa.it (M.C. Mangano), gianluca.sara@unipa.it (G. Sarà).

https://doi.org/10.1016/j.scitotenv.2018.02.106
0048-9697/

1. Introduction

Understanding the abiotic processes that may generate and maintain species occurrence in a focal area is a recognized essential baseline for designing interventions to mitigate biodiversity loss, inform adaptive strategies for a sustainable use of biological resources and more simply explain biotic interaction (Mellin et al., 2016; Bauer et al., 2018). As widely reported in literature, remote sensing of environmental data provides valuable insight into the understanding of processes driving spatial and temporal changes in productivity at sea (Behrenfeld et al., 2006). These data include for instance sea surface temperature (*SST*), chlorophyll-*a* (*CHL-a*) and sea surface currents. However, there is still a poor understanding of the mechanisms that ultimately are responsible for productivity hotspots in the oceans. This knowledge become crucial in a context of multiscale interactions among anthropogenic and climate stressors and to inform future evidence-based sustainable marine resources management strategies (*e.g.*, Pikitch et al., 2004; Dietz et al., 2007; Halpern et al., 2008; Piroddi et al., 2017). The call for sustainability has become mandatory in the last decade recognizing the importance to collect and integrate abiotic and biotic data to disentangle potential resilient ecosystem functions and provision (*e.g.* seafood) to be preserved without threatening socio-economies (Westman, 1977; MA, 2005; Fisher et al., 2009). Management strategies built-up on the knowledge of the driving abiotic interactions may ensure a more tailored planning process more regionalised and spatially explicit as required in the context of the Mediterranean Sea where and when activities such as fishery, aquaculture and tourism are essentially sustained by trophic conditions generating shared productivity hotspots which driven mechanism are unknown (Sarà et al., 2011; Pranovi et al., 2013; Ramírez et al., 2017). To identify the abiotic mechanisms and drivers that generate the species occurrence patterns can be time and resources demanding given the difficulties encountered in collecting, processing, modeling and validating physical data (Mellin et al., 2016). For this reason most of the management actions in place into the Mediterranean Sea have been based on predictions of oceanographic effects on the local trophic conditions and ecological responses at local scale, often performed on mean conditions of hydrodynamic regimes (*e.g.*, monthly, annually; Levi et al., 2003; Bellido et al., 2008; Bacha et al., 2010; Agostini and Bakun, 2002; Martín et al., 2012; Basilone et al., 2013; Giannoulaki et al., 2013; Quattrocchi et al., 2016; Harrison et al., 2017).

As resulting from the gap of a more regionalized knowledge of the acting abiotic variables and the physical driving mechanisms, rules and legislation mostly designed for other environmental contexts, such as for the Northern European countries (*e.g.*, Common Fishery Policy, CFP; Frost and Andersen, 2006; Lado, 2016), were applied in the Mediterranean Sea resulting inadequate where rather the use of higher resolution data is strongly recommended when dealing with biological and ecological processes (*e.g.*, at least daily-averages or much better hourly; Montalto et al., 2014; Lado, 2016; Sarà et al., 2013). We can use a medical analogy and later translate it into the biological oceanography and ecology: the "actual patient care should be highly individualized, and patient treatment should not be based on the results of broad-scale generalizations, without considering the patient's history, risk factors and other medications" (lit.; Helmuth et al., 2014).

A broad-brush approach could be appropriate if high resolution data lack, but the present-day technology offers dramatic improvement of the temporal and spatial resolution of many types of data needed to feed more tailored regional management strategies based on high resolution environmental data layers. The Malta-Sicily Channel (hereafter referred as MSC; central Mediterranean Sea) represents a good cross-border example: the large local productivity (Fig. 1) supports one among the largest fishing fleet in the Mediterranean basin with high aggregation values of fishing pressure in proximity to productivity hotspots (Eigaard et al., 2016). This area is also under significant pressure from intense marine traffic that includes commercial vessels, tankers (La Loggia et al., 2011), oil and gas extraction plants (Mangano and Sarà, 2017) making it highly vulnerable: a tailored management of local shared resources is urgent. A number of topographic and mesoscale to sub-mesoscale oceanographic features, such as fronts, vortices and upwelling regions, both contribute in controlling the local trophic conditions and maintaining high levels of biodiversity (Lermusiaux and Robinson, 2001; Béranger et al., 2004). This region can be considered as an ecological source and sink for many pelagic and demersal species (*e.g.*, anchovy, young tunas, mackerel, red mullet *etc.*; Fiorentino et al., 2003; Levi et al., 2003; Sarà and Sarà, 2007; Falcini et al., 2015; Consoli et al., 2016) feeding primarily both Italian and Maltese local socio-economies.

This research focuses on the following points: *i*) characterizing the surface circulation in the MSC region; *ii*) characterizing the relationship among surface currents and water quality variables; and, *iii*) identifying the possible causes of the large productivity supporting local economies. For these tasks, we analyze surface current data collected through a network of High-Frequency (HF) radars deployed in the MSC area, supported by an EU Italian-Maltese Transnational Programme (Cohesion Policy 2007–2013), and satellite data products such as MODIS SST and CHL-*a* maps available from the OceanColor web portal (http://oceancolor.gsfc.nasa.gov/), managed by NASA. While the initial CALYPSO objective was to gather data for sea safety purposes, the unprecedented resolution in space and time (3 km and 1 h, respectively) of the near-surface circulation was seen as also useful to provide information to disentangle the interaction among oceanographic factors. This will also be important when building the basal information to tailor dynamically the resource exploitation management (downscaled) plans.

2. Materials and methods

2.1. Study area

Currents contribute to dispersion, transport or retention of nutrients, fish larvae and ichthyoplanktonic products of primary importance in the MSC (Lafuente et al., 2002). In first approximation, circulation in the MSC can be described as a two-layer system: *i*) the upper layer, having an approximate thickness of about 200 m, is occupied by the eastwards flow of Atlantic Water (AW); *ii*) the deep layer is occupied by the saltier Levantine Intermediate Water (LIW) (Rinaldi et al., 2014). Before entering the MSC, the AW splits into two main branches, one flowing to the Tyrrhenian Sea along the northern boundary of Sicily, and a second branch flowing into the Sicily Channel. This second branch also splits following two preferential pathways, namely the Atlantic Ionian Stream (AIS) meandering close to the Sicilian coast, and the Atlantic Tunisian Current (ATC) along the northern coast of Tunisia. AIS and ATC show a seasonal pattern in which the ATC is more pronounced in winter and the AIS is prevalent during summer periods. Additionally, the AIS is closely associated with semi-permanent mesoscale vortex features including the intermittent northward extension of the AIS (NAIS) at the Ionian shelf break, which is most likely driven by the surface density contrast between waters of the Sicilian and the Ionian basins (Béranger et al., 2004; Savini et al., 2009). A schematization of the main circulation features is provided in Fig. 1.

2.2. The CALYPSO radar network: description and validation

The radar network consists of SeaSonde HF radars, deployed in the southeastern part of the Malta-Sicily Channel. Two stations were set up initially in the Malta archipelago at the Sopu Tower (station code: SOPU) and at Ta'Barqat (site code: BARK). The area initially covered was ~4000 km^2 (~2400 km^2 of which measured at least 70% of the time). In August 2012 a third station (site code: POZZ) was added on the Sicilian side at the Pozzallo Harbor in August 2013, which significantly extended the spatial coverage in the area (Fig. 2, right panel).

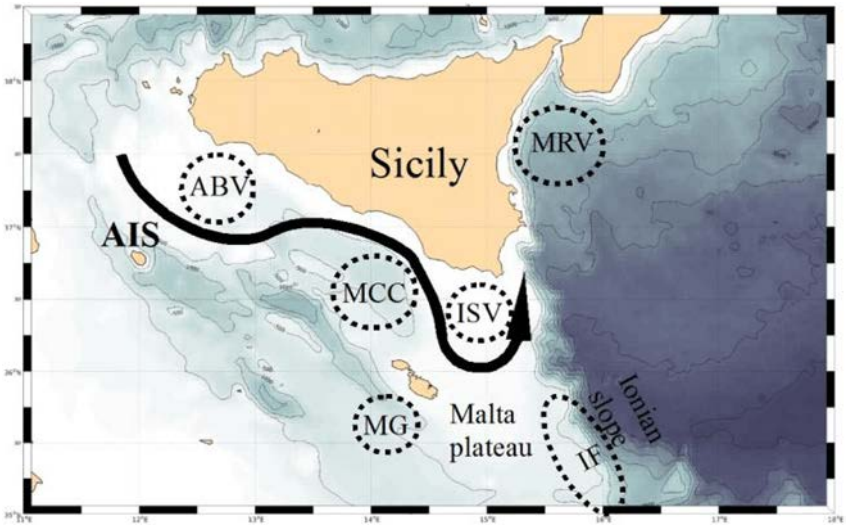

Fig. 1. Simplified vue of the summer circulation in the Sicily Chanel (SC) (Guichoux et al., 2016). Main features include: Atlantic Ionian Stream (AIS), Adventure Bank Vortex (ABV), Maltese Channel Crest (MCC), Ionian Shelf Break Vortex (ISV), Medina Gear (MG), Messina Rise Vortex (MRV), Ionian Front (IF).

The area increased to ~8400 km^2 (~3850 km^2 of which measured at least 70% of the time).

HF radars exploit the Bragg scattering mechanism of a radio frequency signal from rough surfaces to measure the components of sea-surface currents moving towards or away from the transmitter system. In the presence of Bragg-matching waves in the oceans – that is, ocean waves with exactly half the wavelength of a transmitted radio signal – reflection is coherent and generates a strong sea echo return that can be analyzed to determine the distance, direction and velocity of the reflecting surface, from which the radial component of the current can be determined. This process is known as Bragg scattering (Crombie, 1995), and provides the ocean current velocity in the direction of the transmitter (or radial velocity). The reconstruction of sea-surface vector currents from radial velocities is possible when two or more HF radar stations transmit towards the same portion of the ocean (intersection of light grey areas in Fig. 2 left panel), the signals overlap and some geometrical constraints are satisfied. The basic procedure for mapping radial velocities to total currents is described in Gurgel (1994). Error sources in HF radar currents (HF_c) are varied and occur both on radial currents and surface velocity maps (cm s^{-1}). HF radar measurements have been extensively validated in the past, and uncertainty levels of radial and surface current maps are well-known in magnitude and origin (Paduan and Rosenfeld, 1996; Laws et al., 2000; Emery et al., 2004). In particular, uncertainties can be partly explained as "true" measurement errors (instrumental noise or interferences), or associated to intrinsic geophysical variability related to the different sampling strategies (for instance, horizontal and vertical current shears; Chapman and Graber, 1997; Kohut et al., 2012).

Radar currents in the MSC area were validated and compared to more conventional sampling methods, such as Lagrangian buoys (drifters) and vessel-mounted current meters. Drifters were standard holey-sock (Surface Velocity Project) SVP-type drifters, with a holey-sock sail centered at 10 m below the surface and were deployed at selected locations in the MSC region during multiple deployments (December 2012; June, September and October 2013). Additionally, current profiles were acquired at selected locations within the radar coverage over a 2-days period, using a ship-mounted, downlooking 1 MHz Sontek Acoustic Doppler Current Profiler (ADCP). Vertical resolution was set to 1 m, and the sampling frequency to 1 Hz. The accuracy of surface current measurements provided by the CALYPSO monitoring network was found consistent (average *rms* ~ 11 cm s^{-1}) with those from similar installations performed elsewhere (*e.g.*, Cosoli et al., 2010; Kalampokis et al., 2016). The comparison of the radar radial velocities to the radial component of the drifters provided scalar correlation coefficients, r (−), in the range [−0.03, 0.70], with root mean square, *rms* (cm s^{-1}), differences in the range [6.5, 24.45] (Gurgel, 1994; Poulain et al., 2009). For the zonal component r was typically between [0.25, 0.79], *rms* differences between [8.3, 12.1], and improved for the V component, as correlation was found between r = [0.27, 0.89], with *rms* differences in the range [6.6, 9.7]. Moreover, comparison of HF current velocities with ADCP velocities measures over the upper bin cell (3.5 m depth), revealed very good agreement in term of both magnitude (r ~ 0.92) and direction (r ~ 0.90).

As expected, the comparison between radial components of drifter velocity *versus* the radar radial velocities provides a metrics (correlation

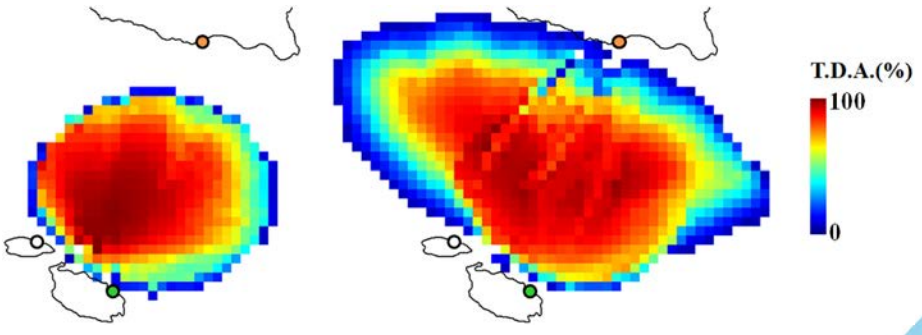

Fig. 2. The three HF stations of the CALYPSO network (SOPU-white, BARK-green and POZZ-orange dots); the temporal data availability (TDA) from January to August 2013 (central panel) of the two HF stations and the TDA of the three HF stations (September–December 2013, right panel). (For interpretation of the references to color in this figure legend, the reader is referred to the web version of this article.)

coefficient r) which spreads over a relatively large range. Low and even negative values are observed; poor correlation depends on a variety of sources, noise level, range to the radar receiver and poor signal-to-noise constraints, pointing errors, and by the different sampling depths.

Differences between the datasets arise partly from the sampling strategies, and partly from the radar system performances (including signal-to-noise decay over range; external noise sources; bearing determination errors). HFR data quality is controlled in first instance by signal-to-noise-ratio (SNR), which typically decays over range; thus, far ranges are more prone to having poorly constrained Doppler lines, which often causes radar measurement errors. At far ranges, the radar cross section (*i.e.*, the dimension of the scattering patch in the ocean) also increases, which in turns determines and increased current variability that the drifter does not capture. Errors in the determination of the direction of arrival of the signal also contribute to a bias in radar currents; this contribution is extremely difficult to quantify because it can be different for different range cells and angular settings. Typical values are in the range $\pm 10°$ but cases are documented in which bearing determination errors are as large as 40°.

Differences between the datasets arise partly from the sampling strategies, and partly from the radar system performances (including signal-to-noise decay over range; external noise sources; bearing determination errors).

The different data sampling strategies act at various levels and introduce a geophysical "noise", that is, processes unresolved at the radar sampling scales as discussed for instances in Chapman and Graber (1997). Indeed, radar currents are wide-area averages over some square kilometers cross-section, they are averaged over time and are representative of ≈1 m depth (at a working frequency of 13.5 MHz), whereas ADCP are point wise measurements at metric vertical resolution and drogued SVP drifter currents used here are representative of 15 m depth.

Cosoli et al. (2010) showed that a large portion of the radar *vs. in situ* current differences in the shallow-water region offshore the Venice lagoon (northern Adriatic Sea) is explained by the wind-driven vertical shear. For the MSC region, the lack of temperature, salinity and wind data with the required temporal and spatial resolutions prevent from a similar quantification. However, even if over a limited number of points, ADCP current profiles provided a preliminary estimate of the vertical shear, which allowed explain some radar-drifter differences in terms of the Ekman-type dynamics. In this sense, the better comparison metrics found for December 2012 deployment is explained in terms of barotropic structure of the water column during the winter period and the lack of summer seasonal stratification.

Finally, it is worth noticing that validation metrics greatly improved when the zonal and meridional velocity components of the surface current vectors were compared to drifter velocities. Indeed, r was in the range [0.53, 0.94] and [0.4, 0.9] for the U and V components, respectively, with *rms* in the range [9.1, 13.9]. These values are consistent with those found in literature and provide a quite robust support this research findings.

2.3. Satellite data: MODIS SST and CHL-a products

CHL-a and *SST* images were retrieved from the OceanColor web portal (http://oceancolor.gsfc.nasa.gov/), managed by NASA. The 8 days aggregated "Level 3 Binned product" was selected in order to remove the bias induced by clouds on higher-frequency product output (1-day average). A total of 46 Level-3 Binned product images (*i.e.*, 8-day long periods), available during the 2013, were compared to the *HFc* data for the same time frame. The Level-3 Binned product is obtained by Level-2 products accumulated over a 8 days temporal window and it is represented in a global equal-area grid with standard bin sizes (of 4.6 km in the present case).

2.4. Data preprocessing and analysis methods

2.4.1. Pre-processing of HFc fields

Hourly HF data were interpolated on a regular latitude-longitude grid and time-averaged over temporal scales compatible with the remote-sense data products (*e.g.*, 8-days averages for the comparison with *CHL-a*/*SST* MODIS products). To avoid biases from missing radar observations, a 70% threshold was applied to the temporal data availability at each HF radar pixel; no temporal interpolation was applied to HF radar while a bicubic interpolation was applied to fill spatial gaps in the radar domain.

2.4.2. Assessment of kinetic energy variables

Total Kinetic Energy (per unit mass), or *TKE*, Eddy Kinetic Energy (*EKE*) and the absolute value of the products between temporal fluctuations u' v' (*ReS*, per unit water density) fields for *HFc* were computed as follows:

$$TKE = \frac{1}{2}\left(\overline{u^2 + v^2}\right)\ (\mathrm{cm2\ s{-}2}); \tag{1}$$

$$EKE = \frac{1}{2}\left(\overline{u'^2 + v'^2}\right)\ (\mathrm{cm2\ s{-}2}); \tag{2}$$

$$ReS = \left|\left(\overline{u' \cdot v'}\right)\right|\ (\mathrm{cm2\ s{-}2}), \tag{3}$$

where, u' and v' are deviations from the time-averaged zonal, u, and meridional, v, velocity components ($\overline{u}$ and $\overline{v}$). The kinetic energy of mean flow (MKE) can be derived as $MKE = TKE - EKE$. Minima and maxima in *EKE* can be associated with energy source or dispersion areas, while *ReS* indicates how energy transfer is mediated by the turbulence. Averages and fluctuations are computed over a 8 day window to match as closely as possible the temporal coverage of *SST*/*CHL-a* data. Time series of spatial averaged kinetic energy variables were finally compared to spatially-averaged maps of *SST* and *CHL-a* in order to determine their correlation.

2.4.3. Spatial correlation analysis between HFc, CHL-a and SST

Spatial correlation maps between sea surface current and *CHL-a* (and *SST*) were determined using a 5 × 5 pixels moving computing kernel. A linear multiple correlation model between the two horizontal components of surface currents (u, set as variable X_1; v, set as variable X_2) and the *CHL-a* (*SST*) variables (set as variable Y) was fitted to the data within the moving kernel. The sign of u and v were assumed positive according to the actual sea current magnitude and direction. The resulting correlation coefficient, r, was associated with the center pixel of the moving kernel. This approach allowed highlighting areas in which significant spatial covariance exists between the surface velocity components, and the selected water quality indicator (pigment value or *SST*).

2.4.4. Spatial correlation analysis between principal components (PC)

A Principal Component Analysis, PCA (Preisendorfer, 1988) was applied to time series of *CHL-a*, *SST* and *HFc* in order to extract the dominant spatial patterns for these variables. Following Richards (1999) eigenvalues and eigenvectors were computed from the covariance matrix. Principal components (PCs) were extracted for *CHL-a*, *SST* and *HFc* using a moving temporal window of different sizes: 32, 64 and 96 days (4, 8, and 12 layers of 8 days averaged data, respectively). The first PC (PC_1) of both *CHL-a* and *SST* (CHL_{PC1} and SST_{PC1}, respectively) was then compared to the correspondent PC_1 of *HFc* (HFc_{PC1}) to determine the spatial correlation pattern between spatially-distributed variables, as described in the next section. The spatial correlation analysis is then carried out similarly to that explained in the previous section. In particular, a simple linear regression model was applied as it involves two variables: using CHL_{PC1} (or SST_{PC1}) and HFc_{PC1} as inputs.

3. Results

3.1. Sea surface currents variability

The sequence of monthly-averaged current maps in the MSC (Fig. 3) confirms the presence of an energetic jet, associated with the AIS, in the central part of the Channel, with average currents reaching 30–40 cm s^{-1}, directed towards SSE as exiting into the Ionian Sea. Additionally, it shows a persistent mesoscale anticyclonic (clockwise) eddy, bounded by the AIS current. This circulation scheme presents a seasonal pattern in which the AIS flow shifts closer to Malta during summer, while it is displaced from coast in winter and the mesoscale vortex reverse the coastal mean flow to a NW direction. Similarly to the jet, the mesoscale cyclone follows the AIS seasonal modulation and shifts zonally in the MSC, as also confirmed by the tracks of the drifters deployed in December 2012. The drifter tracks for this deployment (not shown here) evidenced that this eddy almost occupied the entire channel and trapped the drifters in its interior (with a permanence time ranging from 4 to 40 days).

3.2. Kinetic energy analysis

The kinetic energy analysis is important as the areas characterized by low sea current energy are trapping zones in which the *SST* considerably increases and the *CHL*-advection is drastically reduced. Conversely, during periods in which the AIS jet is evident (Fig. 4) maxima *CHL-a* (and minima *SST*) values correspond to areas where *TKE* is very high.

The link among current kinetic energy and water quality variables is of particular interest when the Ionian Shelf Break Vortex (ISV) occurs within the radar coverage. As example, the ISV was clearly observable between December 2012 and January 2013. Spatial distributions of *TKE*, *EKE* and *ReS* at different temporal aggregation windows (30, 15, 6 and 1 days; Fig. 5) show the vortex in the area. Of course, the vortex eye acts as a trapping area.

Values of *TKE* ~150 cm^2 s^{-2} were observed at the center of the eddy feature (Fig. 5), and are up to one order of magnitude smaller than values observed in the boundary regions where the AIS is predominant (*TKE* ~1100 cm^2 s^{-2}). Similar results were found when comparing *EKE* and *ReS* in the interior and at the borders of the mesoscale eddy: spatially-averaged values were ~40 and ~130 cm^2 s^{-2} for *EKE* inside and outside the vortex respectively; values for spatially-averaged *ReS* were ~70 cm^2 s^{-2} (in the interior domain) and 240 cm^2 s^{-2} outside the vortex.

The temporal evolution of spatial-domain averaged *TKE*, *EKE*, *ReS*, *CHL-a* and *SST* were compared for the entire 2013 year (Fig. 6) to determine the presence of a correlation. This analysis revealed that water quality (*CHL-a* and *SST*) and sea current kinetic variables are mutually related. Kinetic energy variables allow describing the radar currents temporal evolution. *TKE* is larger during winter (January–February) and fall in autumn (October–December); on the contrary, *TKE* minimum values characterize the springer–summer period. Radar *EKE* and *ReS* show higher values in January–April period and lower values in May–October period. Some higher-frequency components, occurring on a monthly time scale, are evident in the radar *EKE* data, that appear also in radar *ReS*, although with a much smaller amplitude then those observed through *EKE*. The time evolution of *CHL-a* and *SST* appear to be negatively correlated each other ($r \sim -0.84$, with *SST* preceding *CHL-a* with a time-lag of 8–16 days approximately). This is particularly clear from April, when *SST* is increasing and reaches its maximum amplitude in August (~25 °C), whereas, on the opposite, *CHL-a* firstly decreases in April reaching its minimum value early in September (~0.06 mg m^{-3}). The comparisons between *CHL-a* and *EKE* and *ReS* reveal a good agreement. *SST* and *TKE* are inversely correlated ($r \sim -0.7$ with *SST* preceding *TKE* with a time-lag of 88 days). A lower time-lags (of 40 days) characterizes the *SST vs. EKE* and *SST vs. ReS* regressions. *CHL-a* is positively correlated to *TKE*, *EKE* and *ReS* ($r \sim 0.74$, ~0.65 and ~0.58 respectively). The time-lag between *CHL-a* and *TKE* is reduced to 40 days; no time-lag is found between *CHL-a* and *EKE*, or *CHL-a* and *ReS*.

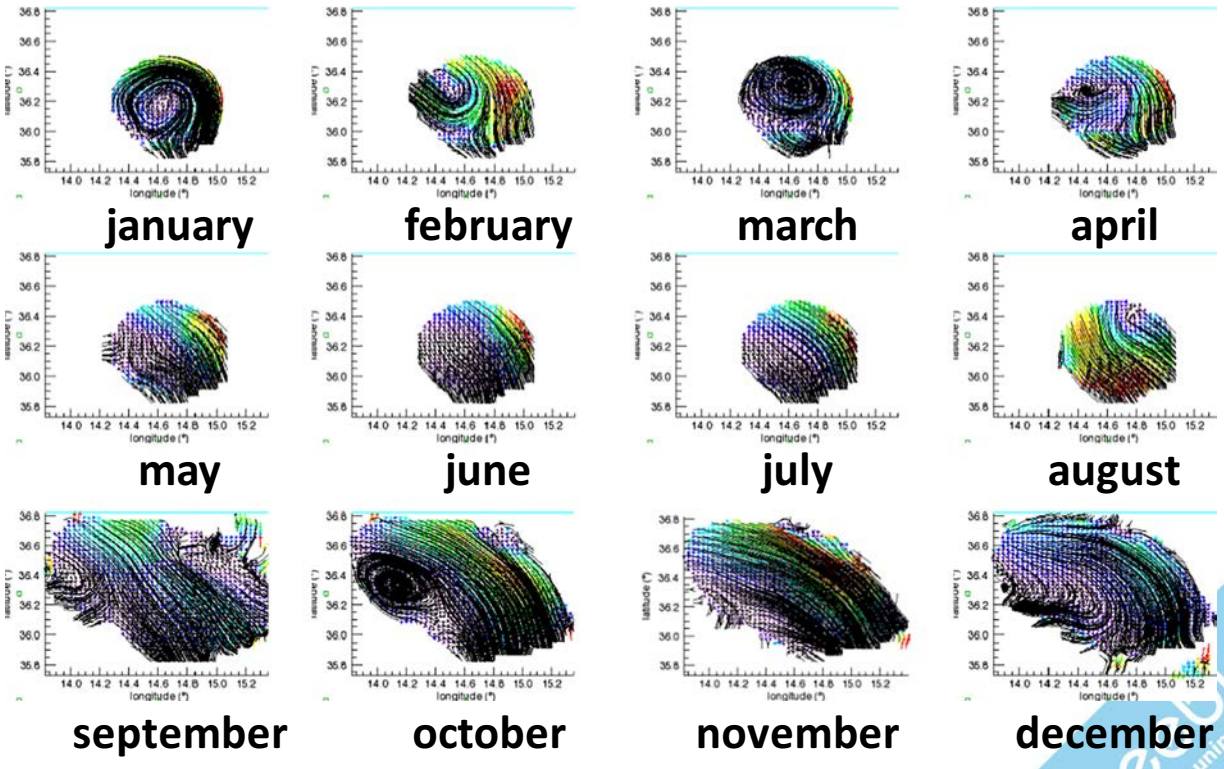

Fig. 3. Sequence of streamlines derived by monthly *HFc* for the time period January–December 2013; the rainbow color ramp is qualitative and it spans from blue (lowest monthly *HFc*) to red (highest monthly *HFc*). (For interpretation of the references to color in this figure legend, the reader is referred to the web version of this article.)

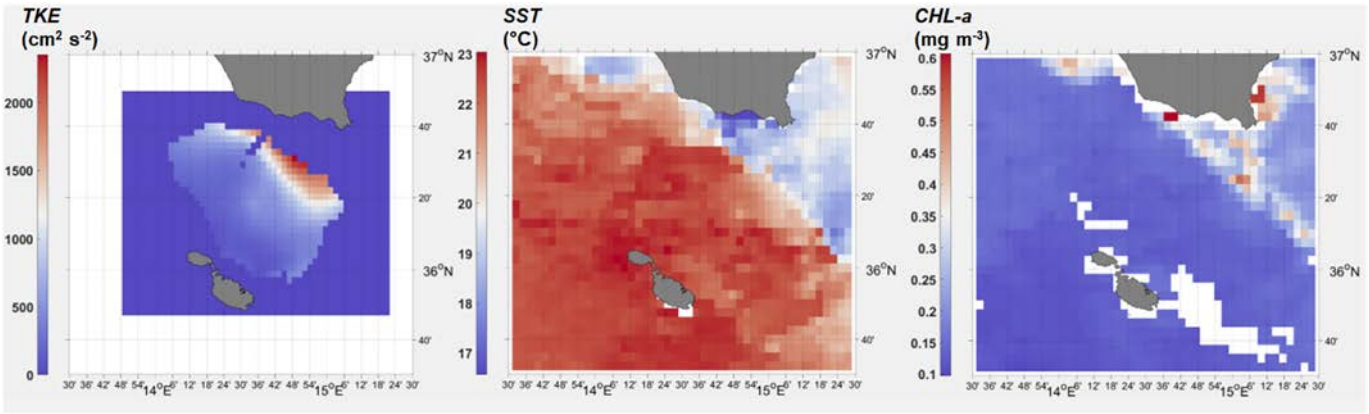

Fig. 4. Maps of *TKE* (left panel), *SST* (central panel) and *CHL-a* (right panel) during a period (*e.g.*, 17 to 24 November 2013) showing a clear AIS shift within the Calypso radar coverage.

3.3. Spatial correlation analysis between HFc, CHL-a and SST

Upwelling events are frequently occurring along the Sicilian coast and are clearly detected by SST and CHL-*a* maps. A macroscopic effect of the AIS in the channel is to detach the CHL-*a* maxima from the coast and advect them offshore or in a SSE direction along its path. In addition, the AIS jet is a cold current, thus, *SST* spatial patterns are expected to be correlated with the sea surface current spatial distributions.

As expected, a high spatial correlation between *HFc* and *CHL-a* (or *SST*) is found, especially when the AIS shift is inside the Calypso radar coverage (Fig. 7), and in particular, often close to the AIS jet edge (Fig. 8).

3.4. Spatial correlation analysis between principal components (PC)

A clear evidence of the spatial correlation between *HFc* currents and water quality variables is observable using the principal component analysis. The first principal component, PC_1 of *CHL-a*, *SST* and HF_C, were examined at different temporal windows, as a time lag between *HFc* and water quality variables can occur even at the mesoscale. Results showed high positive and negative contiguous correlation areas. CHL_{PC1} *vs.* HFc_{PC1} shows maximum $r \sim 0.95$ using a temporal window of 32 days (T_{32}, monthly scale; Fig. 9); SST_{PC1} *vs.* HFc_{PC1} is characterized by maximum $r \sim 0.97$ at 64 days temporal window (bi-monthly scale; Fig. 10). Both correlation patterns for CHL_{PC1} *vs.* HF_CPC_1 and SST_{PC1} *vs.* HFc_{PC1} showed a spatial distribution characterized by fringes where very high positive correlation areas are encircled by areas characterized by very high negative correlations and *vice versa*; this result needs to be further investigated.

4. Discussions

The correct choice of observation scale to disentangle and observe the role of physical oceanography in supporting local mechanisms of

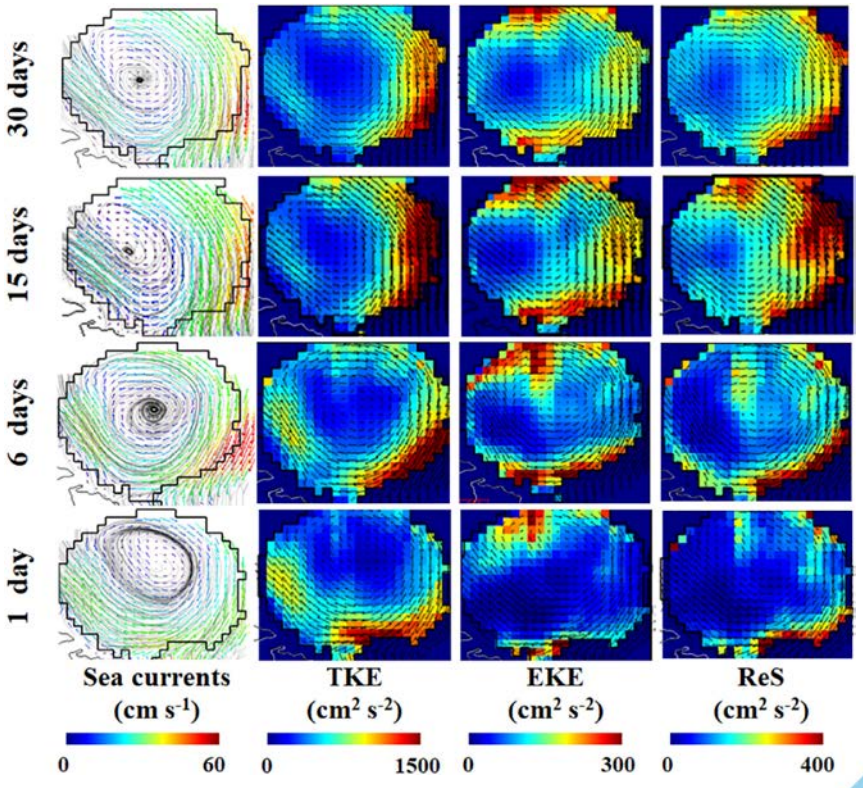

Fig. 5. Spatial distributions of time-averaged radar currents and corresponding *TKE*, *EKE* and *ReS* at different aggregation scales (30, 15, 6 and 1 day).

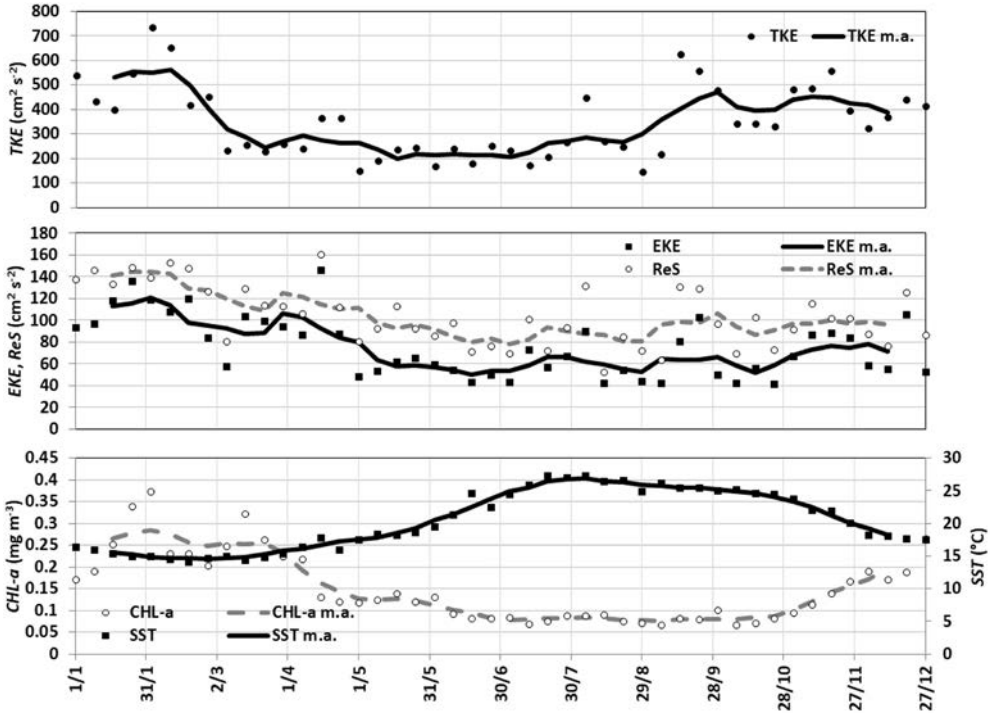

Fig. 6. Time series of spatially-averaged (TDA > 70%) *TKE*, *EKE* and *ReS* from radar currents (upper and middle panels), and corresponding time series of spatially-averaged of *CHL-a* and *SST* data. The time period spans from January to December 2013; over-imposed lines refer to 40 days moving averages.

production should be integrated as layer of primary knowledge when applying combined approach (from climate research, physical oceanography, biogeochemistry, biogeography, and trophic ecology with economical information) to multi-sectorial management of ecosystems (*sensu* Bauer et al., 2018). The detailed statistical analysis performed, within this research, on a novel dataset that comprises sea-surface currents, *CHL-a* and *SST* in the Malta-Sicily Channel, generated spatiotemporal downscaled data. These data represent a knowledge baseline crucial to depict and partially explain abiotic driven mechanisms having effect on bio-ecological process and to integrated when applying integrated approach to inform management measures to may help managers to resolve potential resource management conflicts among counterparts. By integrating this baseline with biological data (*e.g.*, larvae abundance) it may be possible to track patterns of variability generated by physical and biogeochemical parameters (*e.g.*, trapping areas and correlations among kinetic variables) that would otherwise have been lost with more conventional analysis approaches. The understanding of associated biological (at individual level *e.g.* physiology and behavior) and ecological processes (at community and population levels) might also improve the ability to detect local ecosystem resilience phenomena and promote a more sustainable exploitation of marine resources (*sensu* Sustainable Development Goal 14: Conserve and sustainably use the oceans, seas and marine resources; Cormier and Elliott, 2017; Singh et al., 2017). The knowledge of physical driven mechanisms could also help to plan maritime activities in a more adaptive and proactive way also addressing new research avenues in fisheries science (Cash et al., 2003; Barange et al., 2014; Hoegh-Guldberg and Bruno, 2010; Tommasi et al., 2017; Miller et al., 2017). The high resolution data provided in the present analysis allowed a spatial and temporal explicit contextualization of processes generated by specific oceanographic events that may influence the management choice in a context of dynamical adaptation (*e.g.*, Miller et al., 2017). HF radar

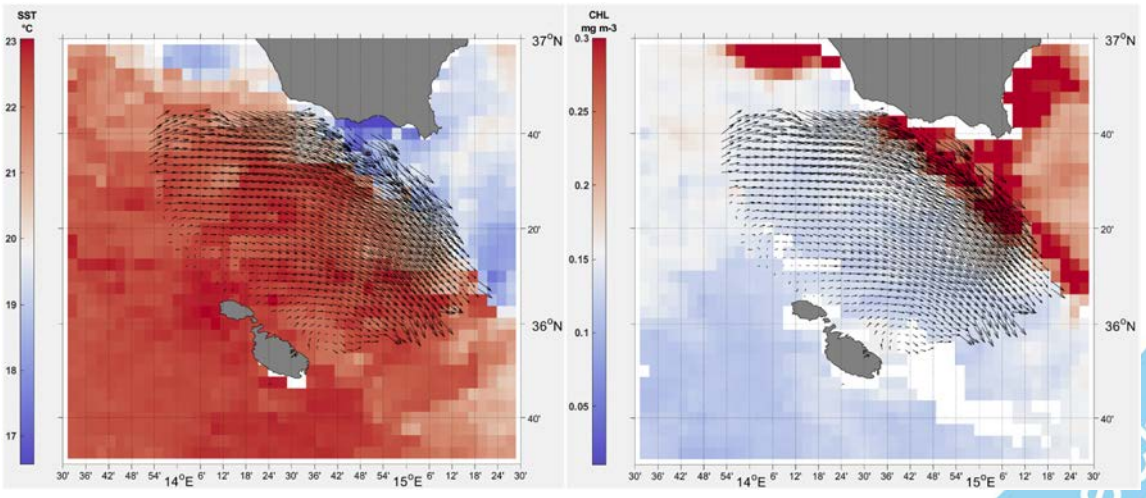

Fig. 7. *HFc* velocity vectors (black arrows) overimposed to *SST* (left panel) and to *CHL-a* (right panel) spatial distributions, during a period in which the AIS is within the Calypso radar coverage.

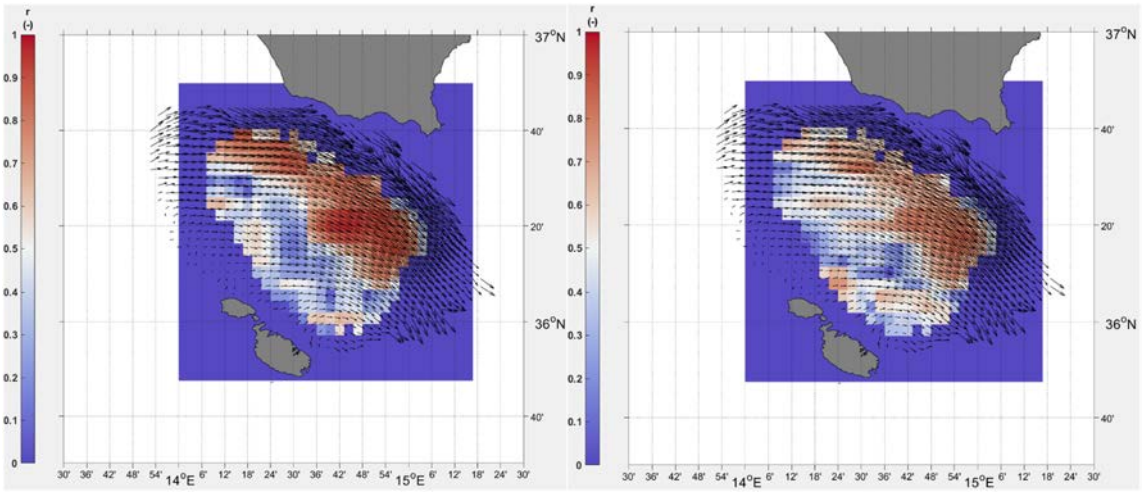

Fig. 8. Maps of spatial correlation between *HFc* velocity *versus* SST (left panel) and *CHL-a* (right panel) during a period in which the AIS shifts is within the Calypso radar coverage.

currents evidenced the dynamics of main circulation features, such as the AIS jet in the central part of the Channel and the mesoscale cyclonic eddy, and provided details on their seasonal variability, the energy balances and the zonal shift between within the MSC region. The gathered evidence may be integrate both phenomenological (*i.e.*, envelope models, ecological niche models or correlative species distributions models; Wiens et al., 2009; Cheung et al., 2013b) and mechanistic (Kearney and Porter, 2009; Sarà et al., 2013; Montalto et al., 2014) models commonly used to predict the distribution of marine species under current and future scenarios of environmental change (Cheung et al., 2013a; IPCC, 2014; Blanchard et al., 2017). They utilize basal quantitative data to derive spatially and temporally-explicit predictions of future species distributions and areas of potential reproductive vulnerability. Thus, within the Mediterranean Sea context, their ability essentially depends on the data quality and quantity of (*i*) basal food-web variables such as chlorophyll-*a* as a proxy of marine ecosystem productivity and as an expression of food availability for secondary consumers (Sheridan and Bickford, 2011; Maureaud et al., 2017) and (*ii*) water mass temperature which is a main driver of organismal metabolism (Kooijman, 2010) above all in ectotherms such as most marine species.

The availability of high-resolution data (*e.g.*, *CHL-a* and *SST*) may provide more elements for a correct resource management reducing the risk of planning and exert human activities at sea when harsh climate events occurs (Payne et al., 2016). Extreme events are expected to increase in frequency in the future and downscaled information may help, as for example, in regulating the fishing pressure selectively reducing the likelihood to incur in resource collapse and the consequent rebounds on local economies (Whitney et al., 2017; Blanchard et al., 2017).

The correlations among variables here detected (evident correlation between currents *versus CHL-a* and *SST* suggesting the importance of current advection in controlling their spatial distributions) will have stronger potential implications in the MSC one among the Mediterranean geographic area where many pelagic species such as European anchovies (*Engraulis encrasicolus*) and other similar small pelagic species such as the *Sardina aurita* and European pilchard (*Sardina pilchardus*) spend most of the lifespan, from eggs to adults (Martín et al., 2012; Falcini et al., 2015). The length in days of larval stages and the total reproductive outputs of these species are strongly influenced by the oceanographic patterns (Olivar and Shelton, 1993; Lloret et al., 2000) which control the local food availability (*e.g.*, floating organisms, *i.e.*, plankton; Falcini et al., 2015) and thermal profiles of upper parts of the water columns exploited by larvae, juveniles and adults (Martín et al., 2012; Quattrocchi et al., 2016). Such life history traits are reference

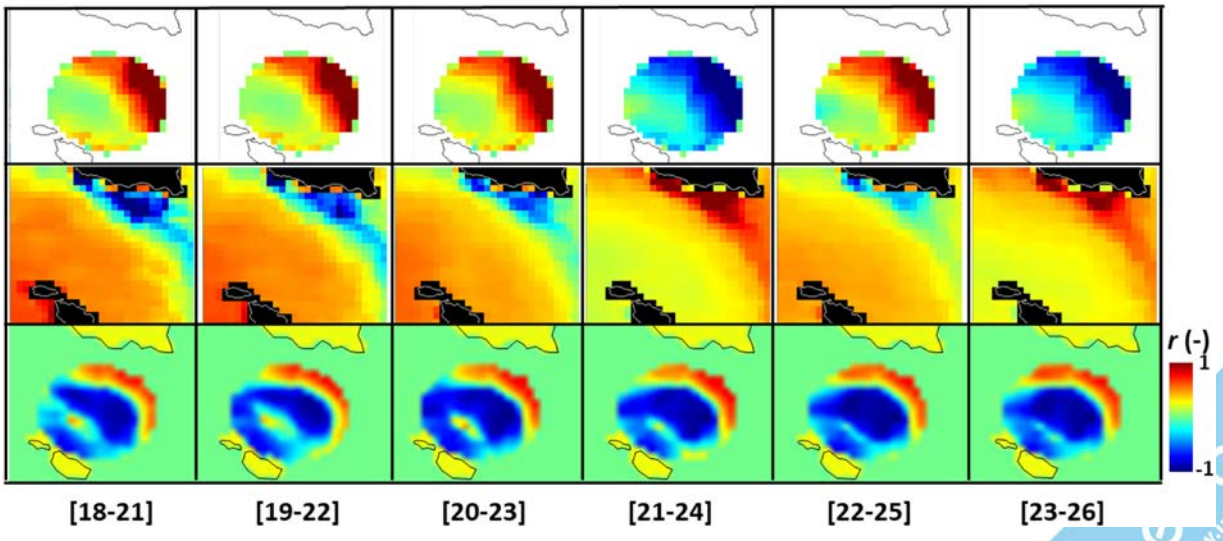

Fig. 9. HFc_{PC1} (upper panels), CHL_{PC1} (central panels) and *r* of the CHL_{PC1} *vs.* HFc_{PC1} relationship (lower panels) calculated using a moving temporal window (size 32 days – T_{32}) during the selected temporal windows (within the brackets periods encompassed within each temporal window are indicated).

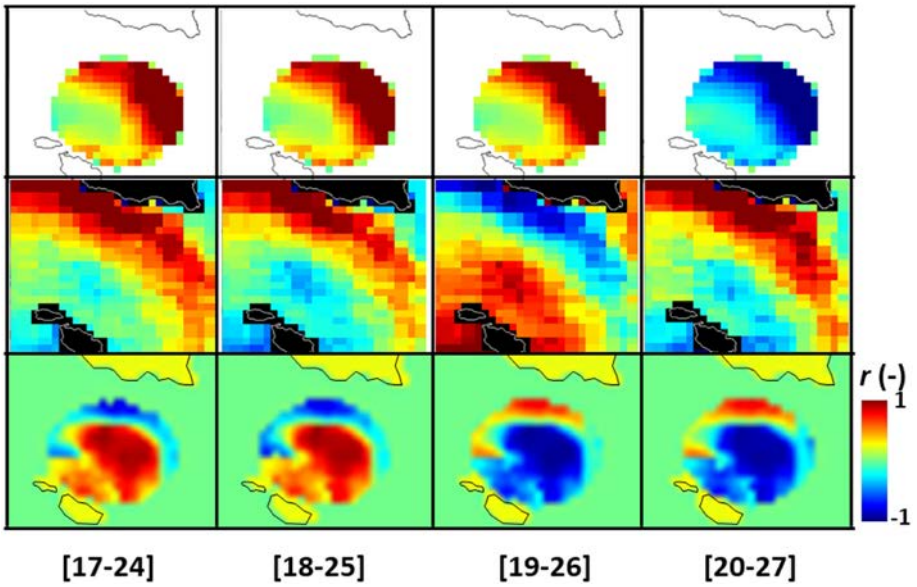

Fig. 10. HFc_{PC1} (upper panels), SST_{PC1} (central panels) and *r* of the SST_{PC1} *vs.* HFc_{PC1} relationship (lower panels) calculated using a moving temporal window (size 64 days – T_{64}) during the selected period.

points to estimate the stock reproductive potential and improve the understanding of stock dynamics; fecundity represents the first input-driver of the population dynamics and when coupled with Lagrangian physical-biological models allow us to predict species dispersal, the identification of likely sink areas at finer spatial resolution (Falcini et al., 2015) and the persistence degree of wild populations. Persistence is an essential component of predictive forecasts of future status of commercial stocks (Munroe et al., 2012), and one of the most important population traits for the efficient creation of dynamic ecosystem-based management plans. Many biological events are efficiently cross-controlled in ectotherms by temperature and food availability (here expressed by *CHL-a*) such as, the planktonic larval duration time which sensitively changes with temperature as predicted from metabolic theory (O'Connor et al., 2007) and with the amount of food which when available over the half-saturation threshold (Holling, 1959; Sarà et al., 2013) can buffer stressful effects due to temperature change.

CHL had a temporal trend related to *EKE* and *ReS* and inversely correlated to *SST*. The spatial correlation analysis allowed quantifying the agreement between patterns of currents and water quality variables, suggesting the importance of relationships between these common patterns and phytoplankton transport at surface. The spatial correlation analysis repeated on CHL_{PCA1}, SST_{PCA1} and HFc_{PCA1} (at monthly, bi-monthly and seasonal scales) highlighted high positive and negative correlations (characterized by higher absolute values at the intermediate scale, $r \approx 0.97$). Both CHL_{PCA1} *vs.* HFc_{PCA1} and SST_{PCA1} *vs.* HFc_{PCA1} correlations showed an interesting spatial distribution characterized by fringes that needs to be further investigated.

The here highlighted peculiar swirling areas (characterized by minima *TKE*, *EKE* and *ReS* values in their eyes), never measured before in this area with such a high precision in the space and time, play the crucial role as a "trapping zone" with significant rebounds on biology and ecology of species spending the life span there. Such trapping zone may help in explaining why the MSC zone is particularly rich in pelagic species gametes and the high temporal resolution data may help in improving spatial management providing spatiotemporal variable dynamic measures (Giannoulaki et al., 2013; Bonanno et al., 2014). The MSC is not only the most fished area in western Mediterranean Sea but also it is an important hot spot of biodiversity (Médail & Quézel, 1999) whereas the risk of accidental oil spill may be high. Indeed this area hosts the second largest oil container harbor in Europe (Augusta, Southern Sicily), the largest oil traffic route in the world (Galgani et al., 2011) and a large number of oil drilling platforms (Mangano and Sarà, 2017). A monitoring network as that based on our HF system, which allows the online acquisition of high-resolution oceanographic data will be crucial to prevent risks on contaminants and to predict the effects of accidental oil spills as well as coastal sewages. Indeed, once spilled, oil often reaches and frequently accumulates on coasts and intertidal habitats, which are crucial for the provision of benefits to humans and the most likely and negatively affected (Sarà et al., 2013; Mangano and Sarà, 2017).

5. Conclusions

The search of spatial correlation between *HFc* and *CHL-a* and *SST* provided valuable information as the *HFc* patterns that can help to determine and forecast particular conditions of nutrients (*e.g.*, *CHL-a*) or *SST* fronts determining favorable conditions for fishing within the MSC and to potentially help in accurately planning human activities at sea avoiding contamination risks. This kind of high resolution datasets allowed to explore possible oceanographic drivers and constraints that have ultimate biological and ecological implications. The possibility to maintain over time devices to collect this types of high-resolution data, can allow a correct monitoring of basal physical variables affecting ecological dynamics. Thus, helping managers and decision makers to suggest and inform tailored measures and strategies in agreement with the reality and not on "averaged" pictures of the environmental variability as often happens as for example in a context of fishery management reducing the existing gap between scientists and decision makers.

Acknowledgments

Surface current data were obtained by the HF radar network installed as part of the CALYPSO project, under partial sponsorship of the EU Operational Programme Italia-Malta 2007-2013. Upon request to the Project Coordinator (Prof. Aldo Drago: aldo.drago@um.edu.mt), radar data can be downloaded after registration to the CALYPSO Professional Data Interface at the following link: www.capemalta.net/calypso. The authors wish to thank Dr. Carmelo Nasello for his help in acquiring ADCP measures.

References

Agostini, V.N., Bakun, A., 2002. 'Ocean triads' in the Mediterranean Sea: physical mechanisms potentially structuring reproductive habitat suitability (with example application to European anchovy, *Engraulis encrasicolus*). Fish. Oceanogr. 11, 129–142.

Bacha, M., Moali, A., Benmansour, N.E., Brylinski, J.M., Mahe, K., Amara, R., 2010. Relationships between age, growth, diet and environmental parameters for anchovy (*Engraulis encrasicolus* L.) in the Bay of Bénisaf (SW Mediterranean, west Algerian coast). Cybium 34 (1), 47–57.

Barange, M., Merino, G., Blanchard, J.L., Scholtens, J., Harle, J., Allison, E.H., Allen, J.I., Holt, J., Jennings, S., 2014. Impacts of climate change on marine ecosystem production in societies dependent on fisheries. Nat. Clim. Chang. 4, 211–216.

Basilone, G., Bonanno, A., Patti, B., et al., 2013. Spawning site selection by European anchovy (*Engraulis encrasicolus*) in relation to oceanographic conditions in the Strait of Sicily. Fish. Oceanogr. 22, 309–323.

Bauer, B., Meier, H.E., Casini, M., Hoff, A., Margoński, P., Orio, A., ... Tomczak, M.T., 2018. Reducing eutrophication increases spatial extent of communities supporting commercial fisheries: a model case study. ICES J. Mar. Sci. https://doi.org/10.1093/icesjms/fsy003.

Behrenfeld, M.J., O'Malley, R.T., Siegel, D.A., McClain, C.R., Sarmiento, J.L., Feldman, G.C., Milligan, A.J., Falkowski, P.G., Letelier, R.M., Boss, E.S., 2006. Climate-driven trends in contemporary ocean productivity. Nature 444 (7120), 752.

Bellido, J.M., Brown, A.M., Valavanis, V.D., Giráldez, A., Pierce, G.J., Iglesias, M., Palialexis, A., 2008. Identifying essential fish habitat for small pelagic species in Spanish Mediterranean waters. Hydrobiologia 612 (1), 171.

Béranger, K., Mortier, L., Gasparini, G.P., Gervasio, L., Astraldi, M., Crépon, M., 2004. The dynamics of the Sicily Strait: a comprehensive study from observations and models. Deep-Sea Res. II 51 (4), 411–440.

Blanchard, J.L., Watson, R.A., Fulton, E.A., Cottrell, R.S., Nash, K.L., Bryndum-Buchholz, A., Büchner, M., Carozza, D.A., Cheung, W.W., Elliott, J., Davidson, L.N., 2017. Linked sustainability challenges and trade-offs among fisheries, aquaculture and agriculture. Nature. Ecol. Evol. 1 (9), 1240.

Bonanno, A., Giannoulaki, M., Barra, M., Basilone, G., Machias, A., Genovese, S., Goncharov, S., Popov, S., Rumolo, P., Di Bitetto, M., Aronica, S., 2014. Habitat selection response of small pelagic fish in different environments. Two examples from the oligotrophic Mediterranean Sea. PLoS One 9 (7), 101498.

Cash, D.W., Clark, W.C., Alcock, F., Dickson, N.M., Eckley, N., Guston, D.H., Jäger, J., Mitchell, R.B., 2003. Knowledge systems for sustainable development. Proc. Natl. Acad. Sci. U. S. A. 100 (14), 8086–8091.

Chapman, D., Graber, H.C., 1997. Validation of HF radar measurements. Oceanography 10 (2), 76–79.

Cheung, W.W., Sarmiento, J.L., Dunne, J., Frölicher, T.L., Lam, V.W., Palomares, M.D., Watson, R., Pauly, D., 2013a. Shrinking of fishes exacerbates impacts of global ocean changes on marine ecosystems. Nat. Clim. Chang. 3 (3), 254.

Cheung, W.W., Watson, R., Pauly, D., 2013b. Signature of ocean warming in global fisheries catch. Nature 497 (7449), 365.

Consoli, P., Esposito, V., Battaglia, P., Altobelli, C., Perzia, P., Romeo, T., Canese, S., Andaloro, F., 2016. Fish distribution and habitat complexity on banks of the strait of Sicily (Central Mediterranean Sea) from remotely-operated vehicle (ROV) explorations. PLoS One 11 (12), e0167809.

Cormier, R., Elliott, M., 2017. SMART marine goals, targets and management–is SDG 14 operational or aspirational, is 'life below water'sinking or swimming? Mar. Pollut. Bull. https://doi.org/10.1016/j.marpolbul.2017.07.060.

Cosoli, S., Mazzoldi, A., Gačić, M., 2010. Validation of surface current measurements in the Northern Adriatic Sea from high-frequency radars. J. Atmos. Ocean. Technol. 27, 908–919.

Crombie, D.D., 1995. Doppler spectrum of sea echo at 13.56 mc/s. Nature 175 (1), 681–682.

Dietz, T., Rosa, E.A., York, R., 2007. Driving the human ecological footprint. Front. Ecol. Environ. 5 (1), 13–18.

Eigaard, O.R., Bastardie, F., Hintzen, N.T., Buhl-Mortensen, L., Buhl-Mortensen, P., Catarino, R., Dinesen, G.E., Egekvist, J., Fock, H.O., Geitner, K., Gerritsen, H.D., 2016. The footprint of bottom trawling in European waters: distribution, intensity, and seabed integrity. ICES J. Mar. Sci. 74 (3), 847–865.

Emery, B.M., Washburn, L., Harlan, J.A., 2004. Evaluating radial current measurements from CODAR high-frequency radars with moored current meters. J. Atmos. Ocean. Technol. 21 (1), 1259–1271.

Falcini, F., Palatella, L., Cuttitta, A., Nardelli, B.B., Lacorata, G., Lanotte, A.S., Patti, B., Santoleri, R., 2015. The role of hydrodynamic processes on anchovy eggs and larvae distribution in the Sicily channel (Mediterranean Sea): a case study for the 2004 data set. PLoS One 10 (4), e0123213.

Fiorentino, F., Garofalo, G., De Santi, A., Bono, G., Giusto, G.B., Norrito, G., 2003. Spatio-temporal distribution of recruits (0 group) of *Merluccius merluccius* and *Phycis blennoides* (Pisces, Gadiformes) in the Strait of Sicily (Central Mediterranean). Migrations and Dispersal of Marine Organisms. Springer, Dordrecht, pp. 223–236.

Fisher, B., Turner, R., Morling, P., 2009. Defining and classifying ecosystem services for decision making. Ecol. Econ. 68, 643–653.

Frost, H., Andersen, P., 2006. The common fisheries policy of the European Union and fisheries economics. Mar. Policy 30 (6), 737–746.

Galgani, F., Hanke, G., Werner, S., Piha, H., 2011. MSFD GES technical subgroup on marine litter. Technical recommendations for the implementation of MSFD requirements. JRC Scientific and Technical Report, EUR 25009 EN – 2011 93 pp.

Giannoulaki, M., Iglesias, M., Tugores, M.P., Bonanno, A., Patti, B., De Felice, A., Leonori, I., Bigot, J.L., Tičina, V., Pyrounaki, M.M., Tsagarakis, K., 2013. Characterizing the potential habitat of European anchovy *Engraulis encrasicolus* in the Mediterranean Sea, at different life stages. Fish. Oceanogr. 22 (2), 69–89.

Guichoux, Y., Lennon, M., Thomas, N., 2016. Sea surface currents calculation using vessel tracking data. Proocedings of Maritime Knowledge Discovery and Anomaly Detection Workshop, Ispra 5–6 July 2016.

Gurgel, K.W., 1994. Experience with shipborne measurement of surface current fields by HF radar. IEEE Oceans 94 Conference. 3(1), pp. III-23–III-27.

Halpern, B.S., Walbridge, S., Selkoe, K.A., Kappel, C.V., Micheli, F., D'agrosa, C., Bruno, J.F., et al., 2008. A global map of human impact on marine ecosystems. Science 319 (5865 (2008)), 948–952.

Harrison, D.P., Hinton, M.G., Kohin, S., Armstrong, E.M., Snyder, S., O'Brien, F., Kiefer, D.K., 2017. The pelagic habitat analysis module for ecosystem-based fisheries science and management. Fish. Oceanogr. 26 (3), 316–335.

Helmuth, B., Russell, B.D., Connell, S.D., Dong, Y., Harley, C.D., Lima, F.P., Sará, G., Williams, G.A., Mieszkowska, N., 2014. Beyond long-term averages: making biological sense of a rapidly changing world. Clim. Change Resp. 1 (1), 6.

Hoegh-Guldberg, O., Bruno, J.F., 2010. The impact of climate change on the world's marine ecosystems. Science 328 (5985), 1523–1528.

Holling, C.S., 1959. Some charachteristics of simple types of predation and parasitism. Can. Entomol. 91, 385–398.

IPCC, 2014. In: Core Writing Team, Pachauri, R.K., Meyer, L.A. (Eds.), Climate Change 2014: Synthesis Report. Contribution of Working Groups I, IIand III to the Fifth Assessment Report of the Intergovernmental Panel on ClimateChange. IPCC, Geneva, Switzerland, p. 151.

Kalampokis, A., Uttieri, M., Poulain, P.M., Zambianchi, E., 2016. Validation of HF radar-derived currents in the Gulf of Naples with Lagrangian data. IEEE Geosci. Remote Sens. Lett. 13 (10).

Kearney, M., Porter, W., 2009. Mechanistic niche modelling: combining physiological and spatial data to predict species' ranges. Ecol. Lett. 12 (4), 334–350.

Kohut, J., Roarty, H., Randall-Goodwin, E., Glenn, S., Lichtenwalner, C., 2012. Evaluation of two algorithms for a network of coastal HF radars in the Mid-Atlantic Bight. Ocean Dyn. 62, 953–968.

Kooijman, S.A.L.M., 2010. Dynamic Energy Budget Theory for Metabolic Organisation. Cambridge University Press.

La Loggia, G., Capodici, F., Ciraolo, G., Drago, A., Maltese, A., 2011. Monitoring Mediterranean marine pollution using remote sensing and hydrodynamic modeling. Proc. SPIE 8174, 817416.

Lado, E.P., 2016. The Common Fisheries Policy: The Quest for Sustainability. John Wiley & Sons.

Lafuente, J.G., García, A., Mazzola, S., Quintanilla, L., Delgado, J., Cuttita, A., Patti, B., 2002. Hydrographic phenomena influencing early life stages of the Sicilian Channel anchovy. Fish. Oceanogr. 11, 31–44.

Laws, K., Fernandez, D.M., Paduan, J.D., 2000. Simulation-based evaluations of HF radar ocean current algorithms. IEEE J. Ocean. Eng. 25 (4), 481–491.

Lermusiaux, P.F., Robinson, A.R., 2001. Features of dominant mesoscale variability, circulation patterns and dynamics in the Strait of Sicily. Deep Sea Res. Part 1 Oceanogr. Res. Pap. 48 (9), 1953–1997.

Levi, D., Andreoli, M.G., Bonanno, A., Fiorentino, F., Garofalo, G., Mazzola, S., Norrito, G., Patti, B., Pernice, G., Ragonese, S., Giusto, G.B., 2003. Embedding sea surface temperature anomalies into the stock recruitment relationship of red mullet (*Mullus barbatus* L. 1758) in the Strait of Sicily. Sci. Mar. 67 (S1), 259–268.

Lloret, J., Lleonart, J., Solé, I., 2000. Time series modelling of landings in Northwest Mediterranean Sea, ICES. J. Mar. Sci. 57, 171–184.

MA, 2005. Ecosystems and human well-being: Scenarios. In: Carpenter, S.R., Pingali, P., Bennet, E.M., Zurek, M.B. (Eds.), 2. Millennium Ecosystem Assessment, Island Press, Washington D.C.

Mangano, M.C., Sarà, G., 2017. Collating science-based evidence to inform public opinion on the environmental effects of marine drilling platforms in the Mediterranean Sea. J. Environ. Manag. 188, 195–202.

Martín, P., Sabatés, A., Lloret, J., et al., 2012. Climate modulation of fish populations: the role of the Western Mediterranean Oscillation (WeMO) in sardine (*Sardina pilchardus*) and anchovy (*Engraulis encrasicolus*) production in the north-western Mediterranean. Clim. Chang. 110, 925–939.

Maureaud, A., Gascuel, D., Colléter, M., Palomares, M.L., Du Pontavice, H., Pauly, D., Cheung, W.W., 2017. Global change in the trophic functioning of marine food webs. PLoS One 12 (8), e0182826.

Médail, F., Quézel, P., 1999. Biodiversity hotspots in the Mediterranean Basin: setting global conservation priorities. Conserv. Biol. 13:1510–1513. https://doi.org/10.1046/j.1523-1739.1999.98467.x.

Mellin, C., Mouillot, D., Kulbicki, M., Mcclanahan, T.R., Vigliola, L., Bradshaw, C.J.A., Brainard, R.E., Chabanet, P., Edgar, G.J., Fordham, A.M., Friedlander, A.M., Parravicini, V., Sequeira, A.M.M., Stuart-Smith, R.D., Wantiez, L., Friedlander, A.M., 2016. Humans and seasonal climate variability threaten large-bodied coral reef fish with small ranges. Nat. Commun. 7, 10491. https://doi.org/10.1038/ncomms10491.

Miller, D.D., Ota, Y., Sumaila, U.R., Cisneros-Montemayor, A.M., Cheung, W.W., 2017. Adaptation strategies to climate change in marine systems. Glob. Chang. Biol. https://doi.org/10.1111/gcb.13829.

Montalto, V., Sarà, G., Ruti, P.M., Dell'Aquila, A., Helmuth, B., 2014. Testing the effects of temporal data resolution on predictions of the effects of climate change on bivalves. Ecol. Model. 278, 1–8.

Munroe, D.M., Klinck, J.M., Hofmann, E.E., Powell, E.N., 2012. The role of larval dispersal in metapopulation gene flow: local population dynamics matter. J. Mar. Res. 70, 441–467.

O'Connor, M.I., Bruno, J.F., Gaines, S.D., Halpern, B.S., Lester, S.E., Kinlan, B.P., Weiss, J.M., 2007. Temperature control of larval dispersal and the implications for marine ecology, evolution, and conservation. Proc. Natl. Acad. Sci. U. S. A. 104, 1266–1271.

Olivar, P.M., Shelton, P.A., 1993. Larval fish assemblages of the Benguela Current. Bull. Mar. Sci. 53 (2), 450–474.

Paduan, D., Rosenfeld, L.K., 1996. Remotely sensed surface currents in Monterey Bay from shore-based HF radar (CODAR). J. Geophys. Res. 101 (1), 20669–20686.
Payne, M.R., Barange, M., Cheung, W.W.L., MacKenzie, B.R., Batchelder, H.P., Cormon, X., Eddy, T.D., Fernandes, J.A., Hollowed, A.B., Jones, M.C., Link, J.S., Neubauer, P., Ortiz, I., Queiros, A.M., Paula, J.R., 2016. Uncertainties in projecting climate-change impacts in marine ecosystems. ICES J. Mar. Sci. 73, 1272–1282.
Pikitch, E., Santora, C., Babcock, E.A., Bakun, A., Bonfil, R., Conover, D.O., Dayton, P.A.O., Doukakis, P., Fluharty, D., Heneman, B., Houde, E.D., 2004. Ecosystem-based fishery management. Science 305, 346–347.
Piroddi, C., Coll, M., Liquete, C., Macias, D., Greer, K., Buszowski, J., Steenbeek, J., Danovaro, R., Christensen, V., 2017. Historical changes of the Mediterranean Sea ecosystem: modelling the role and impact of primary productivity and fisheries changes over time. Sci. Rep. 7. https://doi.org/10.1038/srep44491.
Poulain, P.M., Gerin, R., Mauri, E., Pennel, R., 2009. Wind effects on drogued and undrogued drifters in the Eastern Mediterranean. J. Atmos. Ocean. Technol. 26 (1), 144–156.
Pranovi, F., Sarà, G., Franzoi, P., 2013. Valuing the unmarketable: an ecological approach to the externalities estimate in fishing activities. Sustainability 5 (2), 643–653.
Preisendorfer, R.W., 1988. Principal Component Analysis in Meteorology and Oceanography. Mobley, C.D, Elsevier.
Quattrocchi, F., Mamouridis, V., Maynou, F., 2016. Occurrence of adult anchovy in Catalonia (NW Mediterranean) in relation to sea surface conditions. Sci. Mar. 80 (4), 457–466.
Ramírez, F., Afán, I., Davis, L.S., Chiaradia, A., 2017. Climate impacts on global hot spots of marine biodiversity. Sci. Adv. 3 (2), e1601198.
Richards, J.A., 1999. Remote Sensing Digital Image Analysis: An Introduction. Springer-Verlag, Berlin, Germany.
Rinaldi, E., Buongiorno Nardelli, B., Volpe, G., Santolieri, R., 2014. Chorophyll distribution and variabilità in the Sicily Channel (Mediterranean Sea) as seen by remote sensing data. Cont. Shelf Res. 77 (1), 61–68.
Sarà, G., Sarà, R., 2007. Feeding habits and trophic levels of bluefin tuna *Thunnus thynnus* of different size classes in the Mediterranean Sea. J. Appl. Ichthyol. 23 (2), 122–127.
Sarà, G., Kearney, M., Helmuth, B., 2011. Combining heat-transfer and energy budget models predict thermal stress in Mediterranean intertidal mussels. Chem. Ecol. 27 (2), 135–145.
Sarà, G., Palmeri, V., Rinaldi, A., Montalto, V., Helmuth, B., 2013. Predicting biological invasions in marine habitats through eco-physiological mechanistic models: a case study with the bivalve *Brachidontes pharaonis*. Divers. Distrib. 19 (10), 235–1247.
Savini, A., Malinverno, E., Etiope, G., Tessarolo, C., Corselli, C., 2009. Shallow seep-related seafloor features along the Malta plateau (Sicily channel – Mediterranean Sea): morphologies and geo-environmental control of their distribution. Mar. Pet. Geol. 26 (9), 1831–1848.
Sheridan, J.A., Bickford, D., 2011. Shrinking body size as an ecological response to climate change. Nat. Clim. Chang. 1, 401–406.
Singh, G.G., Cisneros-Montemayor, A.M., Swartz, W., Cheung, W., Guy, J.A., Kenny, T.A., McOwen, C.J., Asch, R., Geffert, J.L., Wabnitz, C.C., Sumaila, R., 2017. A rapid assessment of co-benefits and trade-offs among sustainable development goals. Mar. Policy https://doi.org/10.1016/j.marpol.2017.05.030.
Tommasi, D., Stock, C.A., Hobday, A.J., Methot, R., Kaplan, I.C., Eveson, J.P., Holsman, K., Miller, T.J., Gaichas, S., Gehlen, M., Pershing, A., 2017. Managing living marine resources in a dynamic environment: the role of seasonal to decadal climate forecasts. Prog. Oceanogr. https://doi.org/10.1016/j.pocean.2016.12.011.
Westman, W.E., 1977. How much are nature's services worth? Science 197, 960–964.
Whitney, C., Bennett, N., Ban, N., Allison, E., Armitage, D., Blythe, J., Burt, J., Cheung, W., Finkbeiner, E., Kaplan-Hallam, M., Perry, I., 2017. Adaptive capacity: from assessment to action in coastal social-ecological systems. Ecol. Soc. 18 (22(2)).
Wiens, J.A., Stralberg, D., Jongsomjit, D., Howell, C.A., Snyder, M.A., 2009. Niches, models, and climate change: assessing the assumptions and uncertainties. Proc. Natl. Acad. Sci. U. S. A. 106 (2), 19729–19736.